Journal of Hydrology 595 (2021) 126014

Contents lists available at ScienceDirect

Journal of Hydrology

journal homepage: www.elsevier.com/locate/jhydrol

Research papers

Future changes in the Dominant Source Layer of riparian lateral water fluxes in a subhumid Mediterranean catchment

José L.J. Ledesma [a,b,c,*], Guiomar Ruiz-Pérez [d], Anna Lupon [b], Sílvia Poblador [e,f], Martyn N. Futter [c], Francesc Sabater [e], Susana Bernal [b]

[a] Institute of Geography and Geoecology, Karlsruhe Institute of Technology (KIT), Reinhard-Baumeister-Platz 1, 76131 Karlsruhe, Germany
[b] Integrative Freshwater Ecology Group, Centre for Advanced Studies of Blanes, Spanish National Research Council (CEAB-CSIC), Accés a la Cala Sant Francesc 14, 17300 Blanes, Spain
[c] Department of Aquatic Sciences and Assessment, Swedish University of Agricultural Sciences (SLU), P.O. Box 7050, 750 07 Uppsala, Sweden
[d] Department of Crop Production Ecology, Swedish University of Agricultural Sciences (SLU), P.O. Box 7044, 750 07 Uppsala, Sweden
[e] Departament de Biologia Evolutiva, Ecologia, i Ciències Ambientals, Universitat de Barcelona, Av. Diagonal 643, 08028 Barcelona, Spain
[f] Research Group of Plants and Ecosystems, Department of Biology, University of Antwerp, Universiteitsplein 1, 2610 Wilrijk, Belgium

ARTICLE INFO

This manuscript was handled by Marco Borga, Editor-in-Chief, with the assistance of Christian Massari, Associate Editor

Keywords:
Terrestrial–aquatic interface
Hydrological connectivity
Hydrological modelling
Catchment biogeochemistry
Mediterranean climate
Environmental change

ABSTRACT

The 'Dominant Source Layer' (DSL) is defined as the riparian zone (RZ) depth stratum that contributes the most to water and solute fluxes to streams. The concept can be used to explain timing and amount of matter transferred from RZs to streams in forest headwaters. Here, we investigated the potential impact of future climate changes on the long-term position of the DSL in a subhumid Mediterranean headwater catchment. We used the rainfall-runoff model PERSiST to simulate reference (1981–2000) and future (2081–2100) stream runoff. The latter were simulated using synthetic temperature, precipitation, and inter-event length scenarios in order to simulate possible effects of changes in temperature, rainfall amount, and rainfall event frequency and intensity. Simulated stream runoff was then used to estimate RZ groundwater tables and the proportion of lateral water flux at every depth in the riparian profile; and hence the DSL. Our simulations indicated that future changes in temperature and precipitation will have a similar impact on the long-term DSL position. Nearly all scenarios projected that, together with reductions in stream runoff and water exports, the DSL will move down in the future, by as much as ca. 30 cm. Shallow organic-rich layers in the RZ will only be hydrologically activated during sporadic, large rainfall episodes predicted for the most extreme inter-event length scenarios. Consequently, terrestrial organic matter inputs to streams will decrease, likely reducing catchment organic matter exports and stream dissolved organic carbon concentrations. This study highlights the importance of identifying vertical, hydrologically active layers in the RZ for a better understanding of the potential impact of future climate on lateral water transfer and their relationship with surface water quality and carbon cycling.

1. Introduction

Riparian zones (RZs) link terrestrial and aquatic ecosystems (Johnson and McCormick, 1979; Swanson et al., 1982) and exert a major control over water and solute transfer to forest headwaters worldwide (McDowell et al., 1992; Luke et al., 2007; Bernal et al., 2015; Musolff et al., 2018). The growing consensus on the importance of RZs for catchment hydrology and biogeochemistry has been translated into an increasing number of studies focusing on the processes that regulate the transfer of water and solutes from RZs to streams (Schwab et al., 2016; Laudon and Sponseller, 2018; Weyer et al., 2018). However, a general, mechanistic, cross-ecoregion understanding of how forest RZs transfer matter to adjacent streams remains elusive.

The 'Dominant Source Layer' (DSL) is defined as the RZ depth stratum that contributes the most to water and solute fluxes to streams and it has been recently proposed to explain timing and amount of matter transfer from riparian soils to surface waters in forest headwaters across ecoregions (Ledesma et al., 2018a). The DSL idea is derived from the

Abbreviations: RZ, riparian zone;; DSL, dominant source layer.

* Corresponding author at: Institute of Geography and Geoecology, Karlsruhe Institute of Technology (KIT), Reinhard-Baumeister-Platz 1, 76131 Karlsruhe, Germany.

E-mail address: jose.ledesma@kit.edu (J.L.J. Ledesma).

https://doi.org/10.1016/j.jhydrol.2021.126014
Received 14 July 2020; Received in revised form 11 December 2020; Accepted 17 January 2021
Available online 28 January 2021
0022-1694/© 2021 The Author(s). Published by Elsevier B.V. This is an open access article under the CC BY-NC-ND license (http://creativecommons.org/licenses/by-nc-nd/4.0/).

'control points' concept (Bernhardt et al., 2017), which moves beyond classical 'hot spots' and 'hot moments' (McClain et al., 2003) by integrating both transport and biogeochemical phenomena. The DSL provides a conceptual framework for testable hypotheses on the importance of localized riparian processes on stream hydrology and biogeochemistry (Ledesma et al., 2015, 2018b; Blackburn et al., 2017).

The identification of the DSL position in the riparian vertical profile can be inferred from the relationship between the RZ groundwater table and stream runoff (Seibert et al., 2009). This relationship is characteristic of most forest catchments within Mediterranean (Lupon et al., 2016), boreal (Rodhe, 1989; Seibert et al., 2009; Bishop et al., 2011), and temperate (McDonnell et al., 1998; McGlynn and McDonnell, 2003) ecoregions. Laterally flowing water traversing the RZ picks up the chemical signal corresponding to the depth of its flow path across the RZ, and then transfers it to the stream in corresponding proportions (Bishop et al., 2004). This phenomenon is known as the transmissivity feedback mechanism and has been used to explain water and solute mobilization to streams by lateral flow exports that increase during precipitation events as RZ groundwater table rises and water enters highly conductive riparian layers (Lundin, 1982; Rodhe, 1989; Bishop et al., 2004). Thus, identifying hydrologically active layers in the RZ (i.e. DSLs) is relevant to assess and understand stream water quality in forest and other semi-natural headwater catchments.

Temperature and precipitation ultimately control the vertical position of the DSL at both long (i.e. annual and inter-annual) and short (i.e. precipitation event) temporal scales. For instance, future wetter conditions in boreal regions will promote a shift of the DSL towards upper riparian layers and, consequently, predominant lateral flow paths from RZs to streams will connect more organic-rich strata to the aquatic environment (Ledesma et al., 2015). In the Mediterranean ecoregion, warmer and drier projected conditions for the future (IPCC, 2013) might have the opposite effect; the DSL could move down to deeper, more mineral-rich riparian strata. This change, together with the expected significant reduction in stream runoff under increased aridity (Pascual et al., 2015), could accentuate the disconnection between groundwater and soil organic layers (Butturini et al., 2003), and potentially reduce dissolved organic matter inputs to streams. At the same time, expected changes in precipitation patterns, including both larger precipitation events and longer dry spells, complicate our ability to predict the importance of sporadic hydrological activation of shallow organic-rich layers for organic matter transfer, as well as the extent to which typical runoff generation processes will be altered during exceptionally large storms (Lana-Renault et al., 2014). A better mechanistic understanding of climate-induced changes in predominant riparian water flow paths and their characteristic DSL is thus essential for assessing future climate impacts on stream water quantity and quality in Mediterranean forest catchments.

The objective of the present study was to investigate the potential impact of future changes in temperature and precipitation patterns on the long-term position of the DSL in a subhumid Mediterranean catchment. We used the rainfall-runoff model PERSiST (Precipitation, Evapotranspiration and Runoff Simulator for Solute Transport; Futter et al., 2014) and a combination of synthetic temperature and precipitation scenarios to explore the influence of warmer and drier conditions on stream runoff and the position of the DSL. Inter-event length scenarios were also applied to explore the potential importance of extreme precipitation events on both stream runoff generation and the hydrological activation of shallow RZ layers. Finally, we compared these model results with empirical measurements of organic matter, carbon, and nitrogen content in the RZ vertical profile to identify potential consequences of changes in the DSL for stream water quality and carbon cycling.

2. Study site

Font del Regàs is a Mediterranean catchment with total drainage area of 15.5 km^2 located in the Montseny Natural Park, NE Spain (41°49′ N, 2°27′ E), ca. 30 km NW from the Mediterranean Sea (Fig. 1). The climate is subhumid Mediterranean with mild winters, wet springs, and dry summers. The catchment is biotitic granite-dominated, its altitude ranges from 405 to 1603 m above sea level, and steep slopes (>50%) are present.

Deciduous European beech (*Fagus sylvatica*) forest and a small proportion of heathlands (*Calluna vulgaris* and *Gramineae*) dominate the upper parts of the catchment and cover, respectively, 38% and 2% of the total area. Evergreen oak (*Quercus ilex*) forest and small proportions of coniferous trees dominate in the lower parts and cover 54% of the catchment. Riparian forest, located in the flat near-stream zones (slope < 10%), covers 6% of the catchment and is composed of a mixture of tree species including black alder (*Alnus glutinosa*), black locust (*Robinia pseudoacacia*), European ash (*Fraxinus excelsior*), and black poplar (*Populus nigra*) (Lupon et al., 2016). There is a negligible proportion of riparian forest in the upper 2.9 km stretch of the stream draining the first 1.8 km^2. In the following 3.7 km, the width of the RZ increases from 5 to 32 m, which leads to a 12-fold increase in the total basal area of riparian trees (Bernal et al., 2015).

3. Material and methods

3.1. Stream runoff, riparian groundwater tables, and riparian soil measurements

We measured stream runoff at a location near the valley bottom of the Font del Regàs catchment draining an area of 13.0 km^2 (Fig. 1). Stream water levels were recorded at 15 min intervals from September 2010 to August 2012 using a pressure transducer (Teledyne Isco, Model 1612) attached to a small manmade wall built on one side of the stream channel. At this location, the streambed is made of pebbles, stones, and rocks. Stream water levels recorded with the pressure transducer were converted to stream runoff through the specific rating curve for the location ($R^2 = 0.98$, $p < 0.001$, $N = 65$, uncertainty < 2%; Bernal et al., 2015; Lupon et al., 2016). High frequency values were integrated into daily data for the two-year period ($N = 719$ days). Stream runoff is denoted by units of mm day^{-1} (or mm year^{-1} where appropriate) throughout the paper.

We selected a well-developed riparian forest area located ca. 500 m downstream from the stream runoff measurement point to measure groundwater tables and to characterize the RZ soil profile (Fig. 1). The selected area has the typical soil (>90% sand, bulk density = 1.09 g cm^{-1}) and vegetation types present in the RZs at Font del Regàs (Bernal et al., 2015; Poblador et al., 2017). There are no permanent tributaries between the stream gauge and the riparian site, and drainage area only increases from 13.0 km^2 to 14.0 km^2 in this stream section. In addition, forest type proportions are marginally changed and stream morphological characteristics (i.e. width, depth, and slope) are very similar along the stretch that separates the two locations. Therefore, we assume that specific (i.e. area-normalized) stream runoff was equivalent at these two points. Further, the riparian area is likely a hotspot for water accumulation and export to the stream because it is relatively flat compared to the rest of the catchment. Indeed, water flow direction along this riparian slope is approximately perpendicular to the stream, even during summer low flow conditions (Fig. 1). Moreover, the riparian area is located within a stream reach that is a net receiver of water from the catchment during base flow conditions (Bernal et al., 2015).

Groundwater levels were recorded at 15 min intervals simultaneously with the stream runoff measurements (September 2010 to August 2012) using a perforated PVC tube equipped with a water pressure transducer (Druck PDCR 1830) located 2.5 m from the stream channel within the selected riparian area. Sub-daily high frequency measurements were averaged into daily values for a total of 664 daily records (sporadic device failure precluded a full time series for the full period). Additionally, groundwater levels were manually measured

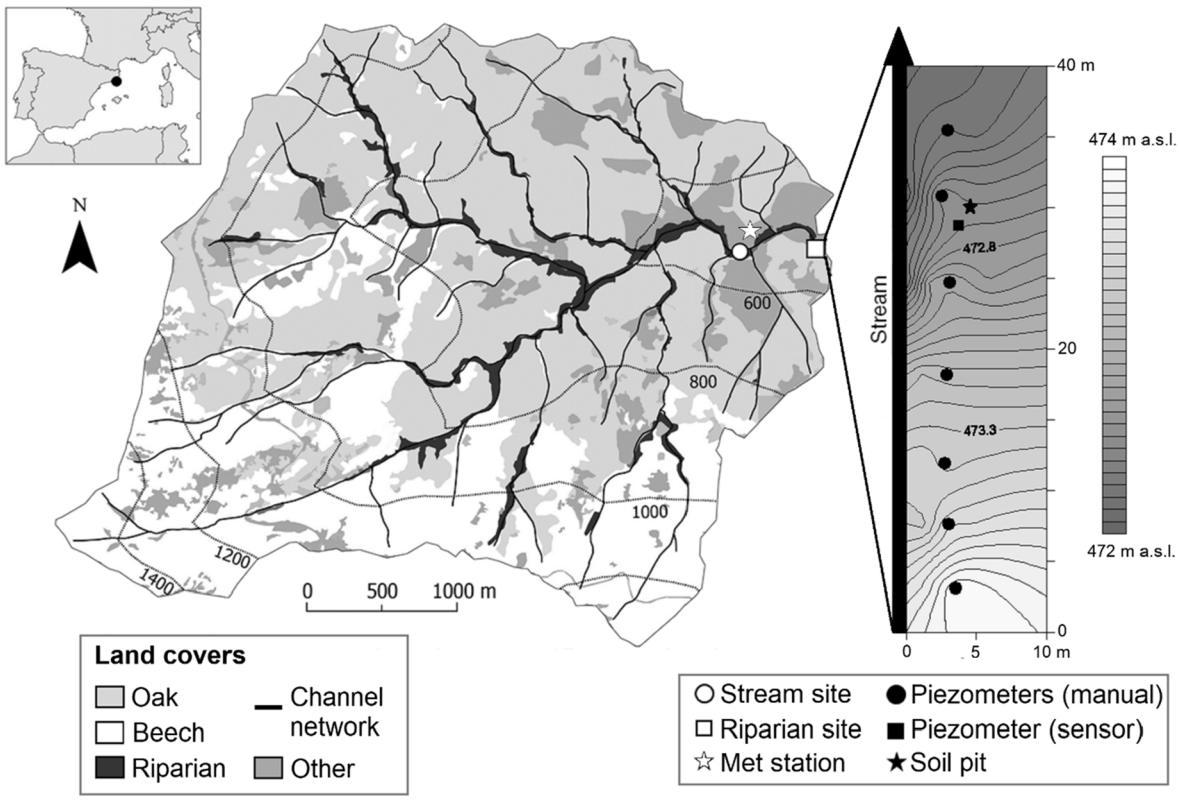

Fig. 1. Map of the Font del Regàs catchment; including channel network (made up by the potential presence of sporadic overland flow paths, intermittent streams, permanent tributaries, as well as the main stream reach), land cover types (including forest types and small proportions of heathlands, coniferous trees, and agricultural fields categorized as 'other'), instrumentations and sampling locations. A schematic representation of the riparian forest area studied, including water pressure head isolines as estimated on August 2010, is also shown. The location of the Font del Regàs catchment within Spain is shown in the inset.

every two weeks during the same period at seven equidistant (ca. 3 m) piezometers installed ca. 2 m from the stream channel along the RZ (Fig. 1). A total of 45 supplementary groundwater table measurements available at each of the seven piezometers were compared with the continuous measurements. Groundwater table dynamics were notably similar in all cases (supplementary Fig. A1), which justified the use of the continuous measurements as representative of the entire riparian forest area.

A soil pit was excavated in June 2018 for physicochemical characterization of the RZ soil profile. The pit was 1.35 m deep and it was located ca. 2 m from the continuous groundwater table measurement location and ca. 4 m from the stream (Fig. 1). We divided the RZ soil profile in ten different strata based on visual differentiation of texture, color, and humidity. For each stratum, three soil samples (i.e. three replicates) were taken and transported in cooling boxes to the laboratory within three hours from collection, where they were kept frozen until physicochemical analyses were made. Soil samples were oven dried at 60 °C until constant weight was reached, sieved, and the < 2 mm fraction was used for physicochemical measurements. Relative soil organic matter content was measured by loss on ignition (450 °C, 4 h). Total soil carbon and nitrogen content were determined on a gas chromatograph coupled to a thermal conductivity detector after combustion at 1000 °C at the Scientific Technical Service of the University of Barcelona.

3.2. Quantification of the Dominant Source Layer

To estimate the DSL at the riparian forest area, we fitted a logarithmic relationship between measured daily groundwater tables and daily stream runoff (Fig. 2). Data were binned to reduce scattering and to weight the relative importance of low versus high stream runoff values, given that base flow conditions were predominant. Hence, daily runoff records were binned at 0.5 cm groundwater table intervals along the total RZ profile depth (set to 2 m) by obtaining the median value within each interval, following the same approach as Grabs et al. (2012).

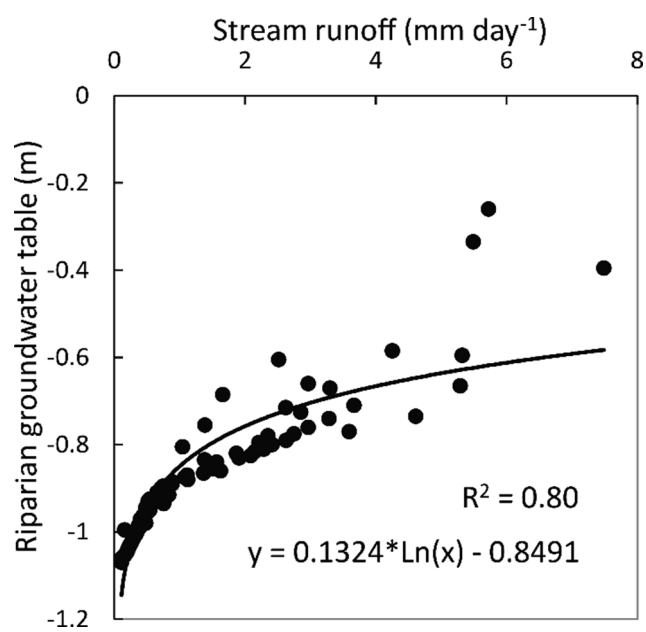

Fig. 2. Relationship between daily groundwater tables at the riparian zone and daily stream runoff at Font del Regàs for the period September 2010 to August 2012 ($p < 0.0001$, $N = 77$). Daily stream runoff records were binned at 0.5 cm groundwater table intervals along the riparian profile.

After this procedure, the final number of observations to fit the logarithmic relationship was 77.

Subsequently, we estimated lateral water fluxes from RZ soil layers to the stream (at a 1 cm resolution) for any given stream runoff by using the logarithmic regression equation and assuming Darcy's law applies, as described by Seibert et al. (2009). In other words, for any given stream runoff, lateral flows at any given RZ soil depth were proportional to the groundwater table – stream runoff curve (Fig. 2), assuming that they only occurred on saturated layers below the groundwater table, i.e. shallow perched flow paths to the stream were neglected. In this way, the DSL can be arbitrarily specified by estimating the relative contribution of each RZ soil depth (at a 1 cm level of resolution) to the total lateral water flux from the entire RZ profile for any given period of time. Thus, the proportion of lateral water flux contribution at every cm in the riparian profile was obtained. This methodology is based on the transmissivity feedback mechanism, conceptualized by Bishop et al. (2004) and mathematically described by Seibert et al. (2009). Following Ledesma et al. (2015), we quantitatively defined the DSL as the RZ depth range contributing 50% of the total lateral water flux. This was done for the two-year calibration period and for the 20-year reference and future simulation periods (see section 3.4) in each corresponding instance. Analogously, we also estimated a DSL responsible for 90% of the total lateral water flux, which represents a more extended estimate of the soil layers contributing to stream runoff. These depth ranges will be hereafter referred to as DSL_{50} and DSL_{90}, respectively.

3.3. Rainfall-runoff model (PERSiST) characterization, calibration, and validation

We used the rainfall-runoff model PERSiST to simulate reference (1981–2000) and future (2081–2100) stream runoff, which was then used to back-calculate RZ groundwater tables and to infer DSLs. PERSiST is a semi-distributed, bucket type model for simulating catchment water fluxes, including stream runoff, at daily time steps (Futter et al., 2014). The model simulates evapotranspiration as a function of temperature, antecedent soil moisture conditions, and catchment vegetation. PERSiST conceptualizes the landscape at four spatial levels. A *catchment* (level 1) is represented as one or more *subcatchments* (level 2). Within each subcatchment, there are one or more *landscape units* (level 3). Finally, each landscape unit is made up of one or more *buckets* (level 4) through which water is routed. Within this flexible framework, the modeller specifies the perceptual representation of the runoff generation process based on a specified number of interconnected buckets within a mosaic of landscape units, namely forest types in the present study. The model requires daily time series of air temperature and precipitation as input data.

We calibrated PERSiST for the two-year period September 2010 to August 2012 (with a prior 8-month warm-up period). To do so, we used daily time series of average air temperature and precipitation measured at a meteorological station located at the valley bottom of Font del Regàs, daily measurements of stream runoff, and a model structure that explicitly included the RZ forest compartment (Fig. 3). This approach was used to successfully simulate and predict future changes in stream runoff at three nested subcatchments along the Font del Regàs stream in a previous study (Lupon et al., 2018). In the present study, a single 13.0 km^2 catchment (a single reach application) was used. We divided the entire catchment in two landscape units: (i) evergreen oak forest (occupying 51% of the total catchment area) and (ii) deciduous beech forest (occupying 49% of the total catchment area). Within each landscape unit, riparian forest occupied 3% of the area and it was accounted for by combining five buckets (upland quick layer, upland soil layer, riparian quick layer, riparian soil layer, and groundwater) in appropriate proportions along the hillslope (Fig. 3), analogously to Lupon et al. (2018). The upland quick and riparian quick layers represented the upper soil stratum that transmit water laterally to the stream only during large precipitation events, in accordance to the DSL concept quantified in Fig. 2.

We improved the Lupon et al. (2018) best parameterization (in terms of model efficiency) to calibrate the single 13.0 km^2 drainage area by manually adjusting the model parameters in order to maximize the values of four performance metrics. The resultant stream runoff simulation was slightly better than the one presented by Lupon et al. (2018), i.e. we obtained a (i) higher Nash–Sutcliffe (NS) efficiency index (Nash and Sutcliffe, 1970), (ii) higher log(NS), (iii) lower relative volume

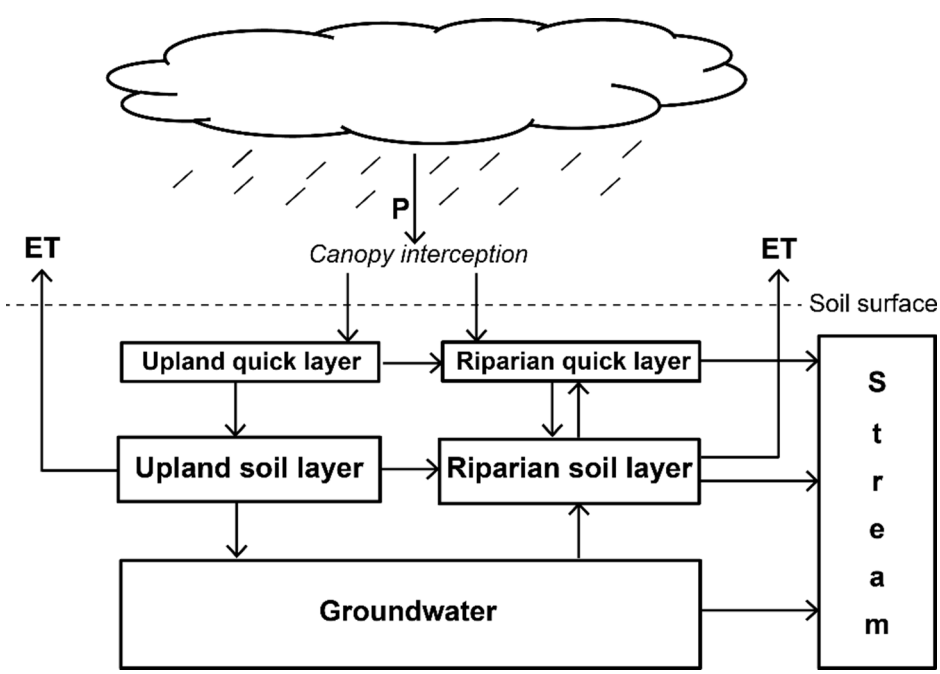

Fig. 3. Conceptual diagram showing water fluxes (arrows) and buckets as configured in the PERSiST application to Font del Regàs in the present study. P is precipitation and ET is evapotranspiration. This configuration was used in the two landscape units in which the catchment was divided (i.e. evergreen oak forest and deciduous beech forest).

differences (RVD) between observed and simulated stream runoff, and (iv) variance of the simulated time series closer to that of the observed data (i.e. the ratio of observed to simulated time series (VAR) was closer to 1). A detailed comparison between model parameters used by Lupon et al. (2018) and model parameters used here can be found in the supplementary material (supplementary Table A1). Further information on model configuration and calibration is available in Lupon et al. (2018).

In order to explore the potential influence of future extreme precipitation events on stream runoff generation, and thereby on DSL positions, we considered two different parameterizations. First, we used the aforementioned manual parameterization, which produced relatively fast rainfall-runoff responses (hereafter referred as to 'fast') under future extreme precipitation events. We then obtained a second model parameterization, derived from the former, which simulated a lower capacity of the system to generate fast rainfall-runoff responses under such extreme events (hereafter referred as to 'slow'). For that, we changed the PERSiST parameter 'time constant' of the upper soil layer in the two landscape units considered. Generally, this parameter defines the residence time of water of a specified soil layer within the specified model structure. At the upper soil layer (defined as 'quick layer' in the present application, Fig. 3), it regulates the immediacy of stream runoff generation during large precipitation events, as we have observed in previous model applications. We increased the value of the 'quick layer' time constant so that (i) the NS efficiency index during the calibration process was maintained within 5% of the original ('fast') parameterization and (ii) the RVD was maintained within 5% (original RVD was 3.1%). These criteria defined our limits of acceptability for behavioural models during calibration (*sensu* e.g. Beven, 2000). Hence, in the slow parameterization, water was transmitted more slowly to the stream during large storms. We expected that this small change in present day parameterizations, i.e. changing the value of one model parameter within the limits of acceptability for behavioural models, might have a disproportionate impact in future rainfall-runoff model simulations that included extreme precipitation events not observed during calibration or the reference period.

We considered previous observations and independent sets of data for validating the model. At Font del Regàs, daily fluctuations in stream runoff can be used as a proxy for daily riparian evapotranspiration dynamics because they are strongly correlated with independent sap-flow measurements from riparian trees (Lupon et al., 2016). Based on these previous empirical evidences, we validated the model by assessing the fit of the linear relationship between monthly mean values of simulated daily riparian evapotranspiration and monthly mean values of observed daily stream runoff fluctuations, for the two-year calibration period (i.e. $N = 24$). We carried out a further model validation by comparing the empirical DSL curve derived from the observed stream runoff measurements with the simulated DSL curves derived from the simulated stream runoff (from fast and slow parameterizations), for the calibration period. As a reminder, for any given period, the DSL curve displays the proportion of lateral water flux contribution at every cm in the riparian profile, which is derived from the characterized RZ groundwater table – stream runoff relationship.

3.4. Future climate scenarios and Dominant Source Layer projections

Because of its longer available time series, we used data from Turó de l'Home, a meteorological station located ca. 6 km southwest from the Font del Regàs meteorological station, to construct daily time series of temperature and precipitation at the study catchment for the reference period 1981–2000. For this, we used the linear regression models ($R^2 > 0.90$, $p < 0.001$, $N = 53$) described by Lupon et al. (2018) that related monthly mean temperature and monthly total precipitation at Font del Regàs and Turó de l'Home stations for the period 2010–2014 (supplementary Fig. A2).

Using 1981–2000 as a baseline, we generated synthetic temperature and precipitation time series by considering the representative concentration pathway (RCP) projection changes for 2081–2100 provided by IPCC for Mediterranean zones. RCP scenarios project an increase in temperature all year round (more pronounced in summer than in winter) that ranges from 0.75 °C in all seasons under the RCP2.5 (percentile 0.25) scenario, to 6 °C in summer and autumn under the RCP8.5 (percentile 0.75) scenario. Precipitation is projected to decrease in April–September, by as much as 35% under the RCP8.5 (percentile 0.25) scenario, while small changes are expected in October–March, including a slight increase of 5% under the RCP2.5 (percentile 0.75) scenario. We applied five scenarios for seasonal changes in both temperature and precipitation that covered the whole range of plausible RCP projections (Table 1), which resulted in an overall change in both temperature and precipitation for the whole 20-year data series for each scenario.

Five inter-event length scenarios were applied by uniformly increasing the duration of the dry spells in the reference period from 0% (no change) to 200%, without changing the overall precipitation amount (supplementary Fig. A3). Hence, the inter-event length was calculated as the difference in days between the last day of a given rainfall event, which defined the start of the dry spell, and the first day of the following event, which defined the end of the dry spell. Rainfall events separated by one day without precipitation were considered independent. Subsequently, the length of the inter-event duration in the reference period was increased by 0, 50, 100, 150 and 200% by delaying the end of the dry spell accordingly. To keep the water volume constant, the total amount of precipitation registered during the days that were originally part of a rainfall event (and subsequently part of the dry spell) was added to the first day of the following rainfall event. These scenarios were meant to represent extreme hydrological conditions, i.e. longer dry spells followed by larger precipitation events (Folwell et al., 2016). Inter-event length scenarios are of interest because the DSL position could vary not only as a consequence of changes in the magnitude of annual precipitation and average temperature, but also because of an increase in the occurrence of hydrological extremes. We combined each of the five inter-event length scenarios considered with each of the five temperature and precipitation scenarios, generating a total of 125 climate scenarios (Table 1).

These 125 synthetic future climatic scenarios, together with the reference scenario, were run in PERSiST using both the fast and slow parameterizations obtained during calibration in order to produce daily time series of stream runoff at Font del Regàs for the corresponding 20-year periods. In a further step, stream runoff was used to back-calculate groundwater tables at the RZ using the estimated RZ groundwater table – stream runoff relationship (Fig. 2). Subsequently, the DSL position was characterized for each of the future scenarios and compared with the DSL position of the reference period using the quantification method described in section 3.2, for both fast and slow parameterization outputs. Relationships between changes in the DSL position and changes in climate variables were established following the scenario-neutral method proposed by Bussi et al. (2016). Briefly, a response surface is created by comparing a variable of interest (here the position of the simulated DSL) with defined climatic stressors (here changes in temperature, precipitation, and inter-event length). Thus, in order to analyze the impact of future climate variable changes on the long-term position of the DSL, changes in the median depth of the DSL_{50} (as the movement up or down with respect to the reference 1981–2000 case) were plotted against overall (20-year) changes in temperature, precipitation, and inter-event length for all future scenarios.

4. Results

4.1. Stream runoff calibration and Dominant Source Layer validation

For the two-year calibration period, average annual precipitation and stream runoff values at Font del Regàs were, respectively, 1087 and 256 mm year^{-1}, and therefore the average annual runoff coefficient was

Table 1
Temperature (T), precipitation (P), and inter-event length (L) (i.e. duration of dry spells) changes applied to the whole reference period (1981–2000) climate data in order to construct future period (2081–2100) scenarios. Each of the five scenarios presented for each climatic variable were combined with each of the five scenarios from the other two variables, generating a total of 125 scenarios. Temperature and precipitation changes covered the whole range of projections from the representative concentration pathway (RCP) scenarios proposed for Mediterranean zones for the period 2081–2100. Inter-event length changes were arbitrarily assigned.

Temperature change (°C)			Precipitation change (%)			Inter-event length change (%)	
Scenario	Dec–May	Jun–Nov	Scenario	Oct–Mar	Apr–Sep	Scenario	Jan–Dec
T1	+0.5	+1.0	P1	−15	−35	L1	0
T2	+1.5	+1.8	P2	−10	−25	L2	+50
T3	+2.5	+3.6	P3	−5	−15	L3	+100
T4	+3.5	+4.2	P4	0	−5	L4	+150
T5	+4.5	+6.0	P5	+5	0	L5	+200

0.24. PERSiST was able to successfully simulate both the temporal pattern and the magnitude of stream runoff (Fig. 4). Model simulations were virtually equivalent between the two parameter sets corresponding to fast and slow runoff response parameterizations, i.e. the difference in performance metrics for the calibration period obtained from these two parameterizations was minimal. NS efficiencies (important to fit high runoffs) and log(NS) (important to fit low runoffs) equalled 0.91 for the fast parameterization, while the values for these two metrics were 0.86 and 0.88, respectively, for the slow parameterization. The model slightly underestimated the total stream discharge by 3.1% (fast parameterization) and 4.6% (slow parameterization). The VAR (important to ensure that observed and simulated series have similar variances) was 0.97 for both parameterizations. The small discrepancy between observed and the two sets of simulated data was mainly associated with two large

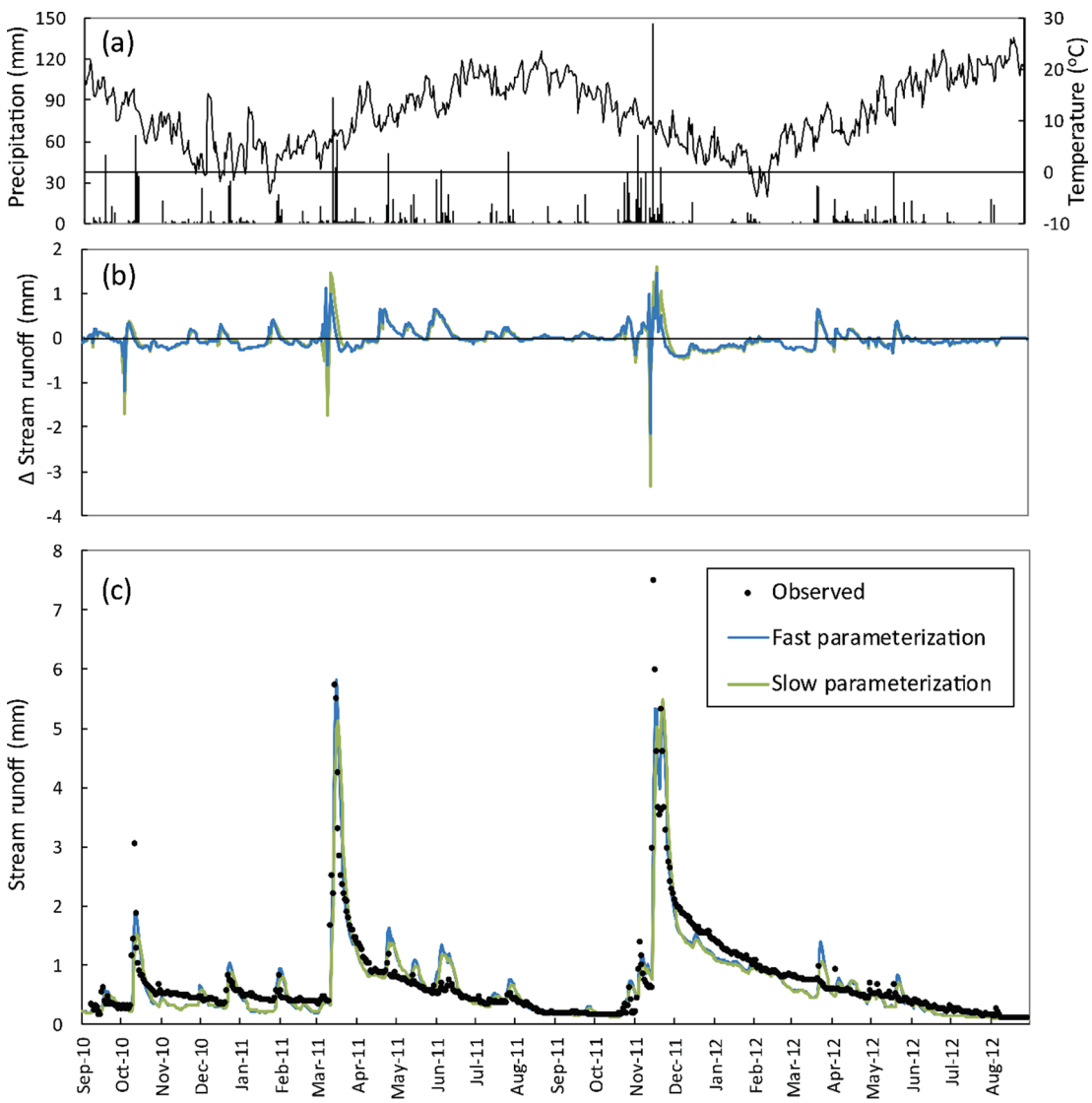

Fig. 4. Time series of (a) precipitation, (b) daily difference (Δ) between observed and simulated stream runoff, and (c) daily observed and simulated stream runoff at the stream measurement location of the Font del Regàs catchment for the calibration period (September 2010 to August 2012). Results are shown for both 'fast' (high potential for fast runoff generation) and 'slow' (low potential for fast runoff generation) model parameterizations. (For interpretation of the references to color in this figure legend, the reader is referred to the web version of this article.)

precipitation events; one in October 2010 (four-day accumulated rainfall of 144 mm) and one in November 2011 (147 mm on November 15) (Fig. 4a, b).

Simulated riparian evapotranspiration and observed diel stream runoff fluctuations (as a proxy for observed riparian evapotranspiration dynamics) were strongly related (linear regression, $R^2 = 0.92$, $p < 0.0001$, $N = 24$), which provided a satisfactory validation of the model (Fig. 5a). Furthermore, there was a good agreement between the DSL curves derived from observed and simulated data, from both the fast and slow parameterizations (Fig. 5b). For the observed data, DSL_{50} was located between 86 and 106 cm below the soil surface (b.s.s.), whereas the simulated DSL_{50} was between 84 and 104 cm b.s.s. for the fast parameterization and between 85 and 105 cm b.s.s. for the slow parameterization. Therefore, the DSL thickness equalled 21 cm in all three cases. Analogously, DSL_{90} was located between 68 and 124 cm b.s.s. and between 65 and 121 cm b.s.s. using the observed data and the simulated (fast and slow) data, respectively (i.e. DSL thickness equalled 57 cm in all three cases).

4.2. Reference and future projections of climate and stream runoff

The reference period (1981–2000) was characterized by an average annual air temperature of 12.9 ± 0.6 °C (average ± standard deviation) and an average annual precipitation of 764 ± 203 mm year^{-1}. The average duration of consecutive days with no rainfall during this period (i.e. average inter-event length) was 4.3 ± 4.7 days and the average daily rainfall event amount was 5.9 ± 10.9 mm day^{-1}. Future (2081–2100) temperature scenarios showed increased annual average values that ranged from 13.6 °C in the less extreme scenario (T1) to 18.1 °C in the most extreme scenario (T5, Table 2). The driest future precipitation scenario (P1) led to an average annual precipitation of 583 ± 171 mm year^{-1}, whereas the value for the wettest scenario (P5) was 786 ± 213 mm year^{-1}, slightly higher than the reference one (Table 2). Future average inter-event length increased from scenario L1 (same as reference) to scenario L2 (12.9 ± 9.4 days). The combination of precipitation and inter-event length scenarios led to a wide range of average daily rainfall event amounts for the future periods, ranging from 4.5 ± 8.8 mm day^{-1} for the combined L1 and P1 scenarios to 25 ± 34 mm day^{-1} for the combined L5 and P5 scenarios (Table 2).

The reference period (1981–2000) showed an average annual simulated stream runoff of 86 and 84 mm year^{-1} for fast and slow parameterizations, respectively. The overall runoff coefficient was 0.11 in both cases, although the inter-annual variation of this parameter was large, ranging from 0.03 to 0.25 (Fig. 6). The distributions of both annual stream runoff and runoff coefficient were very similar between the fast and the slow parameterizations in the reference period. The 125 future (2081–2100) scenarios also produced a large range of annual stream runoff conditions and runoff coefficients; from 12 to 374 mm year^{-1} and from 0.03 to 0.30, respectively. Considering all 125 scenarios, both the slow and the fast parameterization produced similar results at the lower end (i.e. the drier scenarios) of the distributions of both annual stream runoff and runoff coefficient. By contrast, the fast parameterization led to larger annual stream runoff and runoff coefficients than the slow parameterization at the upper end of the distributions (i.e. the wetter scenarios) (Fig. 6). There was a positive relationship between annual precipitation and both annual stream runoff (exponential regression, $R^2 = 0.60$, $p < 0.0001$) and annual runoff coefficient (exponential regression, $R^2 = 0.43$, $p < 0.0001$). However, as precipitation increased, a wide range of possible stream runoff conditions and runoff coefficients were projected (supplementary Fig. A4).

4.3. Reference and future Dominant Source Layer projections

DSL curves derived from future scenarios differed from the DSL curve of the reference period, for both the fast and the slow parameterizations (Table 3, Fig. 7a, b). The depth at which the maximum proportion of lateral water flux occurred shifted from 98 cm b.s.s. in the reference period to 116 ± 13 cm b.s.s. for the combined fast and slow parameterization scenarios in the future. The maximum depth for this descriptor was found at 128 cm b.s.s for six of the future scenarios (in both fast and slow parameterizations). The upper depth that contributed to lateral flow to the stream was located at 61 cm b.s.s. for the reference period, while this depth was deeper for the slow parameterization

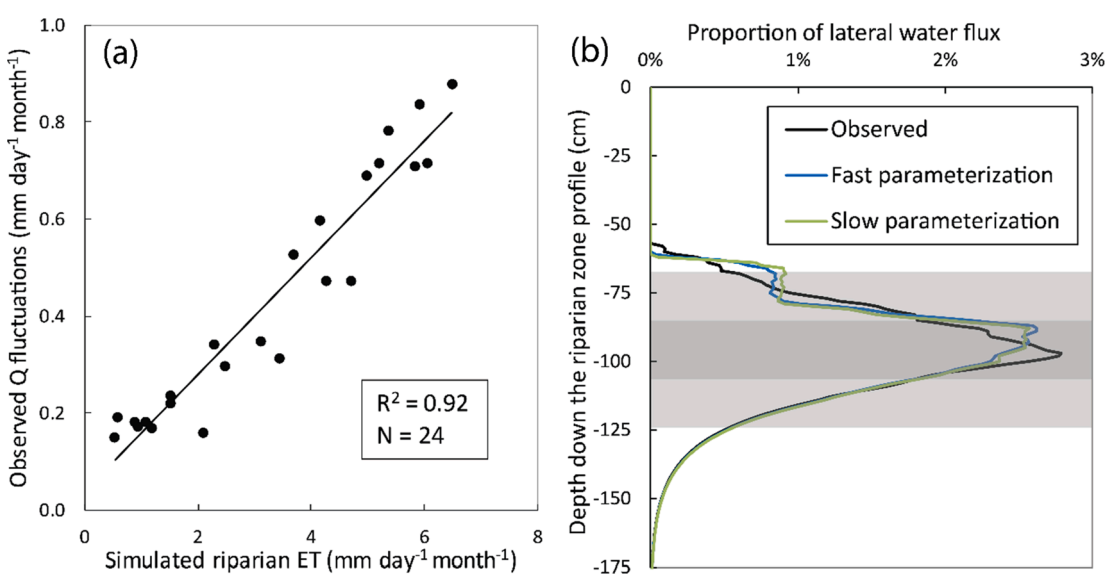

Fig. 5. (a) Relationship between monthly means of simulated daily riparian evapotranspiration (ET) and monthly means of observed diel stream runoff (Q) fluctuations (as a proxy for observed daily riparian evapotranspiration) at Font del Regàs for the calibration period (September 2010 to August 2012). Simulated ET for 'fast' (high potential for fast runoff generation) and 'slow' (low potential for fast runoff generation) model parameterizations was identical. (b) Dominant Source Layer (DSL) curves derived from observed and simulated stream runoffs in relation to riparian zone depth. Light grey depth range represents the DSL_{90} (riparian zone depth range contributing 90% of the total lateral water flux) and the dark grey depth range is the DSL_{50} (riparian zone depth range contributing 50% of the total lateral water flux), as derived from the observed stream runoff data. Both 'fast' and 'slow' model parameterization results are shown in (b). (For interpretation of the references to color in this figure legend, the reader is referred to the web version of this article.)

Table 2
Annual average ± standard deviation (SD) of temperature (T), precipitation (P), and inter-event length (L) (i.e. duration of consecutive days with no rainfall) for reference (1981–2000) and future (2081–2100) scenarios. The range of average ± SD daily rainfall event amounts for reference and future L scenarios is also shown. Each of the five future scenarios presented for T, P, and L were combined with each of the five future scenarios from the other two variables, generating a total of 125 scenarios.

Scenario	Temperature (°C year^{-1})	Scenario	Precipitation (mm year^{-1})	Scenario	Inter-event length (days)	Rainfall event (mm day^{-1})
Reference	12.9 ± 0.6	Reference	764 ± 203	Reference	4.3 ± 4.7	5.9 ± 11
T1	13.6 ± 0.6	P1	583 ± 171	L1	4.3 ± 4.7	4.5 ± 8.8 to 6.0 ± 11
T2	14.5 ± 0.6	P2	638 ± 182	L2	7.6 ± 7.4	8.2 ± 14 to 11 ± 18
T3	15.9 ± 0.6	P3	693 ± 192	L3	10.4 ± 8.7	13 ± 20 to 17 ± 25
T4	16.7 ± 0.6	P4	748 ± 203	L4	11.8 ± 9.1	16 ± 23 to 21 ± 30
T5	18.1 ± 0.6	P5	786 ± 213	L5	12.9 ± 9.4	18 ± 27 to 25 ± 34

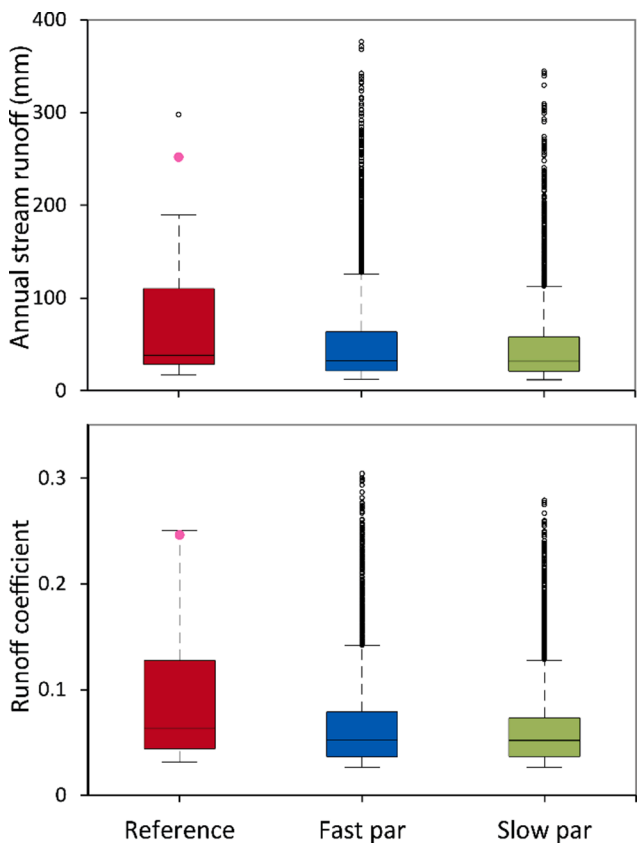

Fig. 6. Distribution of annual stream runoff and annual runoff coefficient values corresponding to all simulated years from the reference period (1981–2000) and the 125 future (2081–2100) scenarios. For the future scenarios, both 'fast' (high potential for fast runoff generation) and 'slow' (low potential for fast runoff generation) model parameterization (par) results are shown. The outputs obtained from both parameterizations for the reference period were very similar and only the results from the fast parameterization are shown. Pink dots represent the corresponding values from the two-year calibration period (September 2010 to August 2012).

scenarios (65 ± 4 cm b.s.s.). The fast parameterization led to the activation of shallower depths in the riparian profile (up to 27 cm b.s.s.) (Table 3, Fig. 7a), specifically for the most extreme inter-event length scenarios (L3 to L5 in Tables 1 and 2).

The upper and lower depths delimiting DSL_{50} for the reference scenario were 87 and 114 cm b. s. s., respectively. These upper and lower depths shifted, respectively, 10 and 15 cm down the riparian profile for the combined fast and slow parameterizations in the future scenarios. By contrast, the thickness of DSL_{50} was similar for both the reference and the future cases, varying between 26 and 36 cm (Table 3). In its turn, DSL_{90} for the reference period was constrained between 76 and 139 cm b.s.s., resulting in a DSL thickness of 64 cm. For the slow

Table 3
Dominant Source Layer (DSL) curve descriptors derived from the reference (1981–2000) and the 125 future (2081–2100) scenarios from both 'fast' (high potential for fast runoff generation) and 'slow' (low potential for fast runoff generation) model parameterizations (par). Model results for the reference period from both parameterizations were equal. For each descriptor, the average ± standard deviation and the range (within parenthesis) of the 125 future scenarios are shown.

DSL curve descriptor	Reference (cm b.s.s.)	Fast par (cm b.s.s.)	Slow par (cm b.s.s.)
Upper contributing depth	61	41 ± 15 (27–75)	65 ± 4 (59–77)
DSL_{90} upper depth	76	51 ± 24 (27–84)	80 ± 3 (72–84)
DSL_{50} upper depth	87	96 ± 7 (84–117)	98 ± 8 (85–117)
DSL_{50} lower depth	114	130 ± 7 (113–142)	129 ± 8 (111–142)
DSL_{90} lower depth	139	149 ± 4 (137–158)	144 ± 4 (135–150)
Max contributing depth	98	116 ± 13 (93–128)	115 ± 13 (92–128)
DSL_{50} thickness (cm)	28	32 ± 2 (26–36)	29 ± 1 (26–32)
DSL_{90} thickness (cm)	64	80 ± 11 (65–96)	65 ± 1 (63–67)

parametrization, the future thickness of DSL_{90} was similar to that simulated for the reference period, yet its upper and lower delimiting depths were, on average, 4 and 5 cm deeper (Table 3). For the fast parameterization, the activation of shallower depths under the most extreme inter-event length scenarios led to the vertical expansion of DSL_{90} along the soil profile (Fig. 7a). For example, scenario T5, P1, L5 (Tables 1, 2) had a DSL_{90} divided into a shallow stratum between 35 and 55 cm b.s.s. and a deeper stratum between 82 and 154 cm b.s.s., which together led to a total thickness of 92 cm.

The DSL position changed in response to changes in climate variables, and the patterns were consistent for both the fast and slow parameterizations (Fig. 8). The position of DSL_{50} rose by only 2 cm only for the wettest scenarios, while it shifted down as much as 28 cm for the driest scenarios. The DSL_{50} position responded similarly to changes in precipitation and temperature; i.e. as the system became warmer and drier, DSL_{50} moved down in the riparian profile in similar proportions (Fig. 8a, d). By contrast, the DSL_{50} position was relatively insensitive to changes in inter-event length (Fig. 8b, c, e, f).

4.4. Characterization of the riparian soil profile

The riparian soil profile consisted of a 10 to 15 cm organic horizon underlain by a semi organic layer with large number of roots down to 35 to 45 cm b.s.s (A horizon). The highest organic matter content (up to ca. 6%) was measured closer to the surface and then decreased with

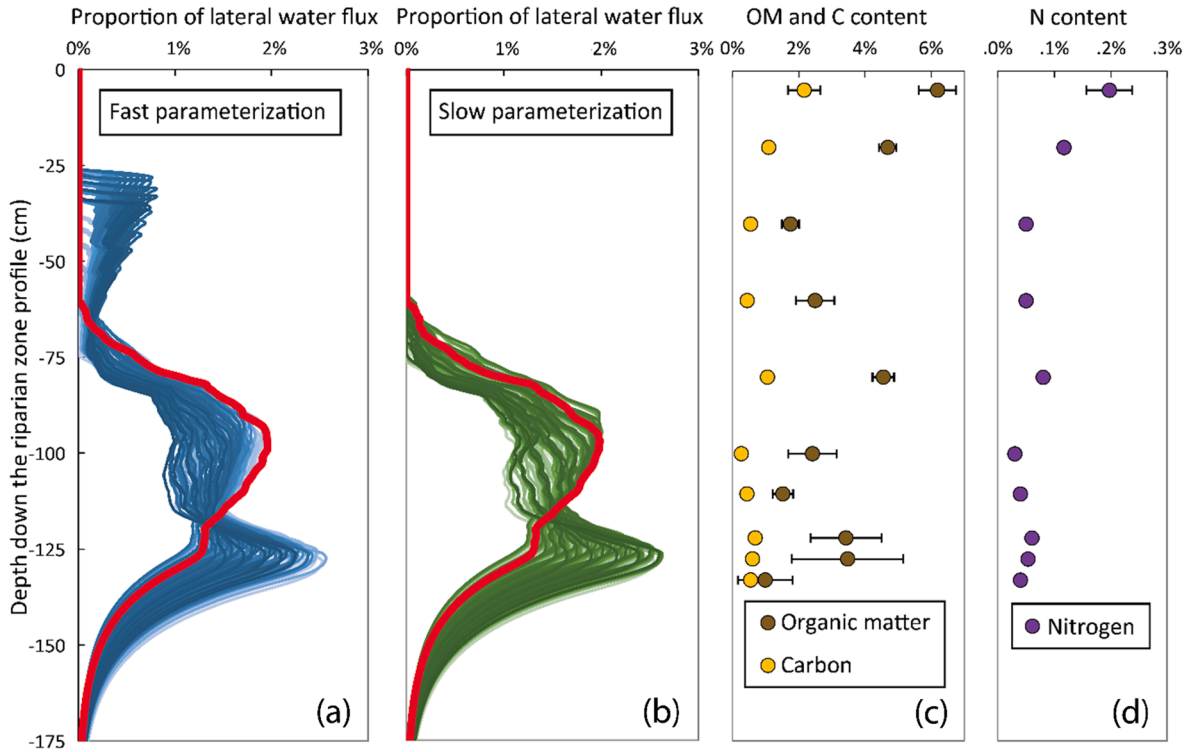

Fig. 7. Dominant Source Layer (DSL) curves derived from reference (1981–2000, thick, red lines) and 125 future (2081–2100) scenarios in relation to riparian zone depth at Font del Regàs. Results are shown for both (a) 'fast' (high potential for fast runoff generation) and (b) 'slow' (low potential for fast runoff generation) model parameterizations. In each case, darker coloured lines correspond to drier scenarios (i.e. higher temperatures, lower precipitations, and higher inter-event lengths), whereas the wetter scenarios are indicated with lighter coloured lines. Vertical distributions of (c) organic matter (OM) and carbon (C) and (d) nitrogen (N) content of a representative riparian soil profile are also shown. For panels (c) and (d), circles represent average values and error bars represent standard deviations of three replicates. (For interpretation of the references to color in this figure legend, the reader is referred to the web version of this article.)

depth down to ca. 1% at 1.35 m b.s.s. (Fig. 7c). Carbon and nitrogen contents followed a similar pattern to the one observed for the organic matter and varied from 0.3% to 2.2% and from 0.03% to 0.2%, respectively (Fig. 7c, d).

5. Discussion

5.1. Overall PERSiST model performance

PERSiST successfully reproduced stream runoff magnitude and dynamics at Font del Regàs, as indicated by all performance metrics (NS, log(NS), RVD, and VAR) and by visual inspection of the hydrographs (Fig. 4c). The overall calibration period was exceptionally wet, which led to an exceptionally high runoff coefficient and high annual stream runoff; yet they were within the plausible reference and future conditions according to our simulations (Fig. 6, supplementary Fig. A4). This could imply that the two parameterizations obtained during the calibration procedure were primarily balanced for wet conditions, which could bias future hydrological projections. However, the calibration period also included typical summer droughts (e.g., only 25 mm of rainfall were recorded in the combined months of June and July of 2012). We argue that the overall exceptionally wet calibration period, which included occasional typical dry conditions, allowed us to calibrate the model under a wide range of stream runoff circumstances, from low base flow to infrequent high stream runoff peaks produced by seldom observed large rainfall events. All in all, we believe that having a set of overall wet and occasional dry conditions was favourable for calibrating the model, simulating future conditions, and developing our main objective, despite the relatively short time series used.

In addition, the exceptionally wide weather conditions encountered during the calibration period ensured that a wide range of RZ groundwater table depths was also captured. This is essential to construct reliable relationships between RZ groundwater tables and stream runoff, which are the basis for subsequent DSL estimations. In Font del Regàs, these two variables were more strongly related (i.e. they showed a higher R^2) than in similar studies conducted in the boreal ecoregion (e.g. Bishop et al., 2011; Ledesma et al., 2016), which further confirms the suitability of our approach. Finally, model validation via comparison of (i) observed stream runoff fluctuations (as a proxy for observed riparian evapotranspiration) and simulated riparian evapotranspiration and (ii) observed and simulated DSLs was satisfactory (Fig. 5). Overall, accurate and validated model simulations were achieved suggesting that the two model parameterizations (fast and slow) were robust and could be used for stream runoff simulations and DSL estimations under reference and future climate scenarios.

5.2. Dominant Source Layer projections and response to climate variable changes

In order to explore the potential response of the DSL to changes in climate, we considered a wide range of climatic conditions based on an ensemble of 125 synthetic climate scenarios that together went beyond the available climate model projections. This approach helped understanding the long-term sensitivity of the DSL position to changes in temperature, total precipitation, and inter-event length, and widely covered potential uncertainties arising from the estimation of future climate variables and model parameterization.

Changes in temperature and total precipitation led to similar changes in the DSL position (Fig. 8), suggesting that these two factors will be equally important in determining the location of important lateral water fluxes in the future. An increase in temperature will likely increase both evaporative demand from the atmosphere and water demand from

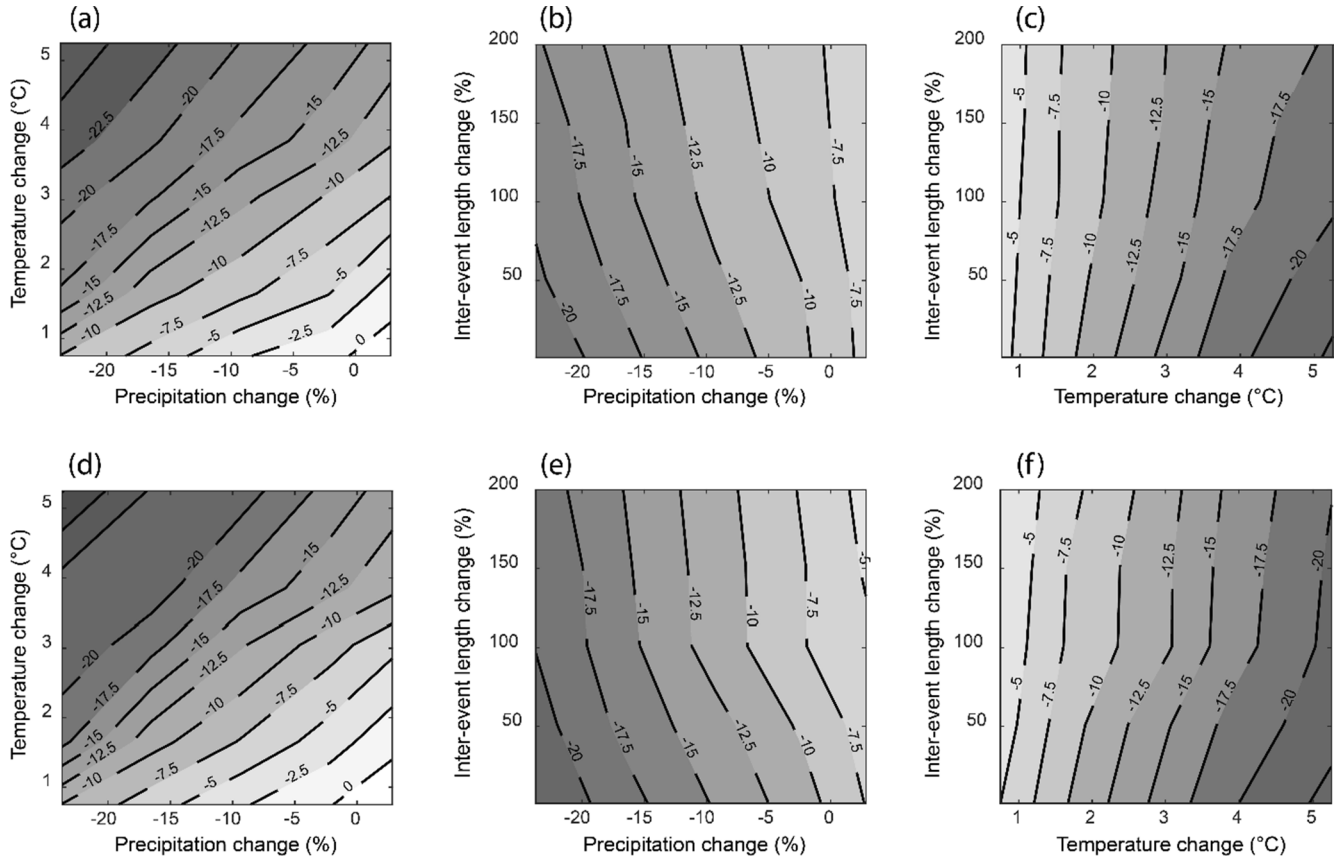

Fig. 8. Future (2081–2100) change in the 50% Dominant Source Layer (DSL_{50}) position with respect to the reference period (1981–2000) as a function of temperature, precipitation, and inter-event length changes, and expressed in centimetres moving down (negative numbers) or up (positive numbers) in the riparian zone profile. The DSL_{50} is defined as the riparian zone depth range contributing 50% of the total lateral water flux. Results are shown for both (a), (b), (c) 'fast' (high potential for fast runoff generation) and (d), (e), (f) 'slow' (low potential for fast runoff generation) model parameterizations.

plants (Wang et al., 2012; Lupon et al., 2018). This increase in evapotranspiration rates in the long-term might lead to a drop in RZ groundwater tables (and thus DSLs) and a consequent decrease in lateral water exports from RZs to streams. Notably, a decrease in precipitation will have a direct effect on the water balance by decreasing water availability, further lowering DSLs and lateral water exports. In turn, a decrease in water availability can also affect plant phenology and growth (Vicente-Serrano et al., 2013), and promote changes in vegetation that might further change evapotranspiration patterns in the RZ (Peñuelas and Boada, 2003; Poblador et al., 2019). Yet, and in a desire for simplicity, we did not consider possible changes in either vegetation cover or evapotranspiration patterns associated with future changes in climatic conditions. Further studies exploring this type of questions would be needed, which could be especially important because the overall effect of climate change on evapotranspiration patterns is a complex issue still under debate (Matheny et al., 2014; Yu et al., 2016; Teuling et al., 2019).

On the other hand, the DSL position was relatively insensitive to changes in inter-event length, for both fast and slow parameterizations, for the overall 20-year periods (Fig. 8). Changes in inter-event length modify the intra-annual distribution of precipitation, which in the most extreme scenarios can lead to (i) periods of very low and deep lateral water transfer from RZs to streams, and (ii) activation of shallow conductive riparian layers in response to large rainfall events. During the overall 20-year period, inter-annual compensatory effects may be concealing these two phenomena, which could partially explain why temperature and total precipitation, but not inter-event length, were the most important climate variables driving long-term trends in the DSL position. Yet, extreme precipitation events could cause sporadic hydrological activations of shallow RZ layers, i.e. organic and A horizons above 35 cm b.s.s. (Poblador et al., 2017), especially for the fast parameterization simulations (Fig. 7a). According to our simulations, the frequency of daily events for which RZ layers above 35 cm b.s.s. will be hydrologically connected to the stream may increase with increasing inter-event length, i.e. from L1 to L5 scenarios (supplementary Fig. A5).

Inter-event length scenarios L2 to L5 included rainfall events larger than 200 mm day^{-1} (and up to 268 mm day^{-1}), which led to a range of associated daily simulated stream runoffs of 37 to 79 mm day^{-1} for the fast parameterization and of 0.1 to 6.4 mm day^{-1} for the slow parameterization. These numbers highlight the discrepancy between the two parameterizations in simulating peaks in stream runoff under exceptionally large precipitation inputs in the future. In light of their different outcomes, the question that arises is whether the fast or the slow parameterizations considered in the present study yield realistic future scenario results. Rainfall events larger than 200 mm day^{-1} have been recorded on several occasions in the NW Mediterranean region (González-Hidalgo et al., 2003; Llasat et al., 2013), and so it is conceivable that they could occur anytime at Font del Regàs (Ledesma et al., 2021). Unfortunately, most of these events do not have associated runoff data from neighboring forest headwater streams because catchments are generally ungauged and no systematic stream runoff measurements are available (Llasat et al., 2013). Consequently, understanding runoff generation during extremely large rainfall events in these systems is challenging and stream runoff peaks appear to be strongly dependent on antecedent soil moisture conditions (Àvila et al., 1992; Bernal et al., 2002; Lana-Renault et al., 2014). This dependency likely led to the wide range of simulated stream runoff conditions and runoff coefficients associated with high overall precipitation at the

annual scale observed here (supplementary Fig. A4). As an example in the context of this discussion, a stream runoff peak of 52 mm day^{-1} was recorded in March 2013 at a forest headwater catchment close to Font del Regàs as a response to a two-day rainfall event of 163 mm (Ledesma et al., 2019). By contrast, the peak in stream runoff recorded at Font del Regàs during the calibration period was 7.5 mm day^{-1} as a response to a two-day rainfall event of 154 mm (Fig. 4).

Thus, we cannot be certain whether the fast or the slow parameterization produced more realistic outcomes and the 'true' answer probably lies somewhere in between. A way to overcome this limitation caused by epistemic uncertainty is to include a wide range of climatic conditions and contrasting model parameterizations in order to cover the range of plausible outcomes, as we have done here. Epistemic uncertainty arises from a lack of knowledge about how to represent a catchment system in terms of both model structure and parameters and may include things that have not yet been perceived as being important, but which might result in reduced model performance when surprise events occur (Beven, 2016). Here we showed that even a minimalist approach to epistemic uncertainty using only a single model and changing a single parameter gave rise to a broad range of system behaviours when, indeed, surprise events (i.e. extremely large precipitation events in future scenarios) were present in the simulations. Such events were missing in the calibration period and the reference scenario, when, by contrast, the fast and slow model parameterizations led to virtually equivalent stream runoff simulations.

Future modelling work could improve on the work presented here by considering specific hydrological processes that could have greater relevance under future climate conditions. For instance, the hydrological activation of shallow RZ layers might be constrained by the actual physical capacity of the soils to first infiltrate and subsequently transfer water laterally to the stream during extreme precipitation events. These events can be associated with rapid runoff generation, overland flow, and destructive flash floods in Mediterranean catchments (Llasat et al., 2013). In its present form, the DSL approach does not directly account for overland flow generation over unsaturated soils as it is based on the static logarithmic relationship between RZ groundwater tables and stream runoff. Moreover, the present approach does not consider the occurrence of reverse hydraulic gradients from the stream to the RZ, which may occur during dry periods in Mediterranean catchments (Butturini et al., 2003; Lupon et al., 2016), and may become more important under drier and warmer conditions. Nevertheless, these dry period-related situations entail very low transfer of both water and solutes, independently on the direction of movement, and are not as critical in the context of matter transfer as hydrological processes associated with extreme rainfall events. Despite these limitations, the approach used here, which combines the use of a well-established rainfall-runoff model and the well-grounded DSL conceptual model, provides a framework for hypothesis testing and prediction that can be useful to infer potential consequences of future climate for the transfer of water and solutes from terrestrial to aquatic ecosystems, and thus for surface water quantity and quality, in Mediterranean headwaters and similar systems located elsewhere.

5.3. Implications for surface water quality

Future changes in the DSL position will likely imply changes in the chemical signal transferred from the RZ to the stream and thus, in surface water quality. At Font del Regàs, the predicted range of change was wide (from a shift up of 2 cm to a shift down of 28 cm) though the general trend shown by most scenarios was towards moving down. For instance, the depth with the maximum contribution to lateral water flux is projected to move down an average of 18 ± 13 cm, from 98 to 116 cm b.s.s. (Table 3) and many scenarios showed the maximum contributing depth as low as at 125 to 128 cm b.s.s. (Fig. 7). Notably, the soil chemistry associated with the deeper RZ layers providing most of the lateral water flux in the future scenarios is different from the RZ layers that contributed the most to the lateral water flux in the reference period. In particular, deeper RZ layers showed lower organic matter, carbon, and nitrogen content, as usually reported for forests soils (Jobbágy and Jackson, 2000, 2001). This suggests that the future drop in the DSL position at Font del Regàs will entail a lower transfer of dissolved organic matter from the RZ to the stream, not only because of the anticipated decrease in water fluxes, but also because dissolved organic carbon (DOC) and nitrogen concentrations in RZ water will likely be lower.

This potential outcome is relevant because dissolved organic matter inputs from terrestrial ecosystems are an important energy source for aquatic organisms and thus future declines could disrupt stream metabolism, ecosystem productivity, and food web structure (Elser et al., 2000; Bernal et al., 2018). At the same time, carbon budgets and cycling could be disrupted by a decrease in lateral carbon exports. To illustrate potential changes in lateral DOC exports and concentrations under future climate conditions, we annually integrated the daily product of simulated lateral flow and measured carbon content in the riparian profile for the most extreme scenarios and compared the resulting lateral DOC export and flow-weighted concentration with the reference scenario. We based these calculations on the fast parametrization simulations, which were more conservative because the sporadic activation of shallow organic-rich RZ layers during large storm events could partially compensate for future declines in lateral DOC exports and concentrations. For this rough approximation, we assumed that (i) measured carbon content pattern in the profile was representative of the entire RZ and did not substantially change over time (Jobbágy and Jackson, 2000), and (ii) measured carbon content was proportional to riparian soil water DOC concentrations (Hope et al., 1997; Evans et al., 2006). The scenario with no changes in inter-event length and the warmest, driest future climate (T5, P1, L1, Table 2) resulted in a 65% lower water transfer, a 71% lower DOC transfer, and a 19% lower annual average DOC flow-weighted concentration. The equivalent scenario with the maximum increase in inter-event length (T5, P1, L5) only moderately compensated for these climatic changes, resulting in a 54% lower water transfer, a 60% lower DOC transfer, and a 12% lower annual average DOC flow-weighted concentration.

These heuristic calculations suggest that, even in those cases for which the activation of shallow hydrological flow paths could offset declines in carbon export, future declines in the DSL will alter carbon cycling and in-stream processes in subhumid and semiarid Mediterranean forest catchments that experience the proposed climate changes by substantially decreasing lateral carbon fluxes (Bernal et al., 2019). Moreover, it is unlikely that rapid and intermittent inputs from shallow flow paths could sustain the ecological status of the aquatic environment in the long-term. Such a pattern of inputs would likely have other undesirable consequences for the stability of stream ecosystems, including high rates of bank erosion and transport of sediments, as well as damage or scouring of stream and riparian biota (Fisher et al., 1982; Ledesma et al., 2019).

6. Conclusions and further investigations

This study combined the DSL concept and the use of climate scenarios in a rainfall-runoff model to estimate future changes in the vertical position of predominant lateral water fluxes from the RZ to the stream in a subhumid Mediterranean catchment. Our model exercise illustrates that small changes in present day calibrations, represented by rainfall-runoff model parameterizations, can have a significant impact on future projections of stream runoff. Two model parameterizations simulated the same stream runoff in the calibration period, but produced significant differences in stream runoff responses under future scenarios with extreme precipitation events. This is the result of epistemic uncertainty, a common limitation in hydrological models and which can only be overcome with more data and information (and hence more measurements, investigations, and understanding) and that should be

treated subjectively based on expert judgment (Beven and Smith, 2015). Here, we attempted to treat uncertainty in this way by using two contrasting behavioural parameterizations together with an ensemble of 125 synthetic climate scenarios, as we consider it to be the most sensible approach for integrating hydrological modelling, climate change projections, and water resources management in catchments worldwide.

We showed that the DSL of riparian lateral water fluxes in Mediterranean headwaters such as Font del Regàs will likely drop down in the future as a consequence of both an increase in average temperature and a decrease in total precipitation. Our simulations suggest that the DSL position is not sensitive to changes in inter-event length, though longer dry spells and larger rainfall events could lead to the sporadic hydrological activation of shallow organic-rich soil layers in the RZ. Overall, these changes in predominant lateral flow paths will lead to (i) declines in lateral water export and in DOC (and likely other organic nutrients) concentrations and exports from RZs to these Mediterranean streams for most of the year, and (ii) an increasing importance of extreme rainfall episodes on annual water balances.

This study highlights that the DSL concept in combination with the use of rainfall-runoff models offer a simple and useful framework to assess stream water quantity and quality in forest headwaters worldwide. This type of approaches can e.g. help to constrain lateral carbon exports from terrestrial ecosystems to inland waters, which is critical to quantify global carbon balances (Tank et al., 2018). Studies of changes in the location of the DSL between wet and dry periods are needed in future applications aiming to investigate finer temporal scale patterns in hydrological processes and runoff generation changes associated with climate variation. The inclusion of vegetation change scenarios associated with climate change as well as a dynamic RZ groundwater table – stream runoff relationship that accounts for potential seasonal variability will also be important to project possible future changes in the water balance more rigorously. In conclusion, an integrative DSL approach is needed for the management of water resources in forest headwater catchments.

CRediT authorship contribution statement

José L. J. Ledesma: Conceptualization, Methodology, Formal analysis, Investigation, Writing - original draft, Writing - review & editing. **Guiomar Ruiz-Pérez:** Methodology, Formal analysis, Writing - review & editing. **Anna Lupon:** Investigation, Resources, Writing - review & editing. **Sílvia Poblador:** Investigation, Resources, Writing - review & editing. **Martyn N. Futter:** Methodology, Writing - review & editing. **Francesc Sabater:** Investigation, Resources. **Susana Bernal:** Conceptualization, Investigation, Resources, Writing - review & editing.

Declaration of Competing Interest

The authors declare that they have no known competing financial interests or personal relationships that could have appeared to influence the work reported in this paper.

Acknowledgments

JLJL was funded by the project RIPARIONS granted by the European Commission through a Marie Skłodowska Curie Individual Fellowship (H2020-MSCA-IF-2018-834363) and by the Spanish Government through a Juan de la Cierva grant (FJCI-2017-32111). AL was supported by the Spanish and Catalan Governments through a Juan de la Cierva (FJCI-2016-28416) and a Beatriu de Pinós (BP-2018-00082) grants. SB work was funded by European Social Funds (FSE) and the Spanish Government through a Ramón y Cajal fellowship (RYC-2017-22643) and the CANTERA project (RTI-2018-094521-B-101). GR was supported by the Swedish Research Council Formas through grant 2018-01820 and by the Swedish government through the project Trees and Crops for the Future (TC4F). We would like to thank Svenja Hoffmeister for valuable assistance with Matlab scripts. The Vichy Catalan Company, the Regàs family, and the Catalan Water Agency (ACA) graciously gave permission for sampling at the Font del Regàs catchment. Finally, we would like to thank five anonymous reviewers for their valuable comments that helped improving the paper.

Appendix A. Supplementary data

Supplementary data to this article can be found online at https://doi.org/10.1016/j.jhydrol.2021.126014.

References

Àvila, A., Piñol, J., Rodà, F., Neal, C., 1992. Storm solute behavior in a montane Mediterranean forested catchment. J. Hydrol. 140 (1–4), 143–161. https://doi.org/10.1016/0022-1694(92)90238-q.

Bernal, S., Butturini, A., Sabater, F., 2002. Variability of DOC and nitrate responses to storms in a small Mediterranean forested catchment. Hydrol. Earth Syst. Sci. 6 (6), 1031–1041. https://doi.org/10.5194/hess-6-1031-2002.

Bernal, S., Lupon, A., Ribot, M., Sabater, F., Martí, E., 2015. Riparian and in-stream controls on nutrient concentrations and fluxes in a headwater forested stream. Biogeosciences 12 (6), 1941–1954. https://doi.org/10.5194/bg-12-1941-2015.

Bernal, S., Lupon, A., Catalán, N., Castelar, S., Martí, E., 2018. Decoupling of dissolved organic matter patterns between stream and riparian groundwater in a headwater forested catchment. Hydrol. Earth Syst. Sci. 22 (3), 1897–1910. https://doi.org/10.5194/hess-22-1897-2018.

Bernal, S., Lupon, A., Wollheim, W.M., Sabater, F., Poblador, S., Martí, E., 2019. Supply, demand, and in-stream retention of dissolved organic carbon and nitrate during storms in Mediterranean forested headwater streams. Front. Environ. Sci. 7 https://doi.org/10.3389/fenvs.2019.0006010.3389/fenvs.2019.00060.s001.

Bernhardt, E.S., Blaszczak, J.R., Ficken, C.D., Fork, M.L., Kaiser, K.E., Seybold, E.C., 2017. Control points in ecosystems: moving beyond the hot spot hot moment concept. Ecosystems 20 (4), 665–682. https://doi.org/10.1007/s10021-016-0103-y.

Beven, K.J., 2000. Uniqueness of place and process representations in hydrological modelling. Hydrol. Earth Syst. Sci. 4 (2), 203–213.

Beven, K., 2016. Facets of uncertainty: epistemic uncertainty, non-stationarity, likelihood, hypothesis testing, and communication. Hydrol. Sci. J.-J. Sci. Hydrol. 61 (9), 1652–1665. https://doi.org/10.1080/02626667.2015.1031761.

Beven, K., Smith, P., 2015. Concepts of information content and likelihood in parameter calibration for hydrological simulation models. J. Hydrol. Eng. 20 (1), 15. https://doi.org/10.1061/(asce)he.1943-5584.0000991.

Bishop, K., Seibert, J., Köhler, S., Laudon, H., 2004. Resolving the Double Paradox of rapidly mobilized old water with highly variable responses in runoff chemistry. Hydrol. Process. 18 (1), 185–189. https://doi.org/10.1002/(ISSN)1099-108510.1002/hyp.v18:110.1002/hyp.5209.

Bishop, K., Seibert, J., Nyberg, L., Rodhe, A., 2011. Water storage in a till catchment. II: Implications of transmissivity feedback for flow paths and turnover times. Hydrol. Process. 25 (25), 3950–3959. https://doi.org/10.1002/hyp.8355.

Blackburn, M., Ledesma, J.L.J., Näsholm, T., Laudon, H., Sponseller, R.A., 2017. Evaluating hillslope and riparian contributions to dissolved nitrogen (N) export from a boreal forest catchment. J. Geophys. Res.-Biogeosci. 122 (2), 324–339. https://doi.org/10.1002/jgrg.v122.210.1002/2016JG003535.

Bussi, G., Dadson, S.J., Prudhomme, C., Whitehead, P.G., 2016. Modelling the future impacts of climate and land-use change on suspended sediment transport in the River Thames (UK). J. Hydrol. 542, 357–372. https://doi.org/10.1016/j.jhydrol.2016.09.010.

Butturini, A., Bernal, S., Hellin, C., Nin, E., Rivero, L., Sabater, S., Sabater, F., 2003. Influences of the stream groundwater hydrology on nitrate concentration in unsaturated riparian area bounded by an intermittent Mediterranean stream. Water Resour. Res. 39 (4) https://doi.org/10.1029/2001WR001260.

Elser, J.J., Fagan, W.F., Denno, R.F., Dobberfuhl, D.R., Folarin, A., Huberty, A., Interlandi, S., Kilham, S.S., McCauley, E., Schulz, K.L., Siemann, E.H., Sterner, R.W., 2000. Nutritional constraints in terrestrial and freshwater food webs. Nature 408 (6812), 578–580. https://doi.org/10.1038/35046058.

Evans, C.D., Reynolds, B., Jenkins, A., Helliwell, R.C., Curtis, C.J., Goodale, C.L., Ferrier, R.C., Emmett, B.A., Pilkington, M.G., Caporn, S.J.M., Carroll, J.A., Norris, D., Davies, J., Coull, M.C., 2006. Evidence that soil carbon pool determines susceptibility of semi-natural ecosystems to elevated nitrogen leaching. Ecosystems 9 (3), 453–462. https://doi.org/10.1007/s10021-006-0051-z.

Fisher, S.G., Gray, L.J., Grimm, N.B., Busch, D.E., 1982. Temporal succession in a desert stream ecosystem following flash flooding. Ecol. Monogr. 52 (1), 93–110. https://doi.org/10.2307/2937346.

Folwell, S.S., Harris, P.P., Taylor, C.M., 2016. Large-scale surface responses during European dry spells diagnosed from land surface temperature. J. Hydrometeorol. 17 (3), 975–993. https://doi.org/10.1175/jhm-d-15-0064.1.

Futter, M.N., Erlandsson, M.A., Butterfield, D., Whitehead, P.G., Oni, S.K., Wade, A.J., 2014. PERSiST: a flexible rainfall-runoff modelling toolkit for use with the INCA family of models. Hydrol. Earth Syst. Sci. 18 (2), 855–873. https://doi.org/10.5194/hess-18-855-2014.

González-Hidalgo, J.C., De Luís, M., Raventós, J., Sánchez, J.R., 2003. Daily rainfall trend in the Valencia Region of Spain. Theor. Appl. Climatol. 75 (1–2), 117–130. https://doi.org/10.1007/s00704-002-0718-0.

Grabs, T., Bishop, K., Laudon, H., Lyon, S.W., Seibert, J., 2012. Riparian zone hydrology and soil water total organic carbon (TOC): implications for spatial variability and upscaling of lateral riparian TOC exports. Biogeosciences 9 (10), 3901–3916. https://doi.org/10.5194/bg-9-3901-2012.

Hope, D., Billett, M.F., Milne, R., Brown, T.A.W., 1997. Exports of organic carbon in British rivers. Hydrol. Process. 11 (3), 325–344. https://doi.org/10.1002/(sici)1099-1085(19970315)11:3<325::aid-hyp476>3.0.co;2-i.

IPCC, 2013. Summary for policymakers. In: Stocker, T.F. et al., (Eds.), Climate Change 2013: The Physical Science Basis, Cambridge University Press, Cambridge, UK.

Jobbágy, E.G., Jackson, R.B., 2000. The vertical distribution of soil organic carbon and its relation to climate and vegetation. Ecol. Appl. 10 (2), 423–436. https://doi.org/10.2307/2641104.

Jobbágy, E.G., Jackson, R.B., 2001. The distribution of soil nutrients with depth: global patterns and the imprint of plants. Biogeochemistry 53 (1), 51–77. https://doi.org/10.1023/a:1010760720215.

Johnson, R.R., McCormick, J.F., 1979. Strategies for protection and management of floodplain wetlands and other riparian ecosystems. In: Proceedings of the Symposium, December 11-13, 1978, Callaway Gardens, Georgia. U. S. Forest Service, Washington Office, General Technical Report (W0-12): 410 pp.

Lana-Renault, N., Nadal-Romero, E., Serrano-Muela, M.P., Alvera, B., Sánchez-Navarrete, P., Sanjuan, Y., García-Ruiz, J.M., 2014. Comparative analysis of the response of various land covers to an exceptional rainfall event in the central Spanish Pyrenees, October 2012. Earth Surf. Process. Landf. 39 (5), 581–592. https://doi.org/10.1002/esp.v39.510.1002/esp.3465.

Laudon, H., Sponseller, R.A., 2018. How landscape organization and scale shape catchment hydrology and biogeochemistry: insights from a long-term catchment study. Wiley Interdiscip. Rev.-Water 5 (2), e1265. https://doi.org/10.1002/wat2.2018.5.issue-210.1002/wat2.1265.

Ledesma, J.L.J., Grabs, T., Bishop, K.H., Schiff, S.L., Köhler, S.J., 2015. Potential for long-term transfer of dissolved organic carbon from riparian zones to streams in boreal catchments. Glob. Chang. Biol. 21 (8), 2963–2979. https://doi.org/10.1111/gcb.2015.21.issue-810.1111/gcb.12872.

Ledesma, J.L.J., Futter, M.N., Laudon, H., Evans, C.D., Köhler, S.J., 2016. Boreal forest riparian zones regulate stream sulfate and dissolved organic carbon. Sci. Total Environ. 560, 110–122. https://doi.org/10.1016/j.scitotenv.2016.03.230.

Ledesma, J.L.J., Futter, M.N., Blackburn, M., Lidman, F., Grabs, T., Sponseller, R.A., Laudon, H., Bishop, K.H., Köhler, S.J., 2018a. Towards an improved conceptualization of riparian zones in boreal forest headwaters. Ecosystems 21 (2), 297–315. https://doi.org/10.1007/s10021-017-0149-5.

Ledesma, J.L.J., Kothawala, D.N., Bastviken, P., Maehder, S., Grabs, T., Futter, M.N., 2018b. Stream dissolved organic matter composition reflects the riparian zone, not upslope soils in boreal forest headwaters. Water Resour. Res. 54 (6), 3896–3912. https://doi.org/10.1029/2017WR021793.

Ledesma, J.L.J., Montori, A., Altava-Ortiz, V., Barrera-Escoda, A., Cunillera, J., Àvila, A., 2019. Future hydrological constraints of the Montseny brook newt (Calotriton arnoldi) under changing climate and vegetation cover. Ecol. Evol. 9 (17), 9736–9747. https://doi.org/10.1002/ece3.v9.1710.1002/ece3.5506.

Llasat, M.C., Llasat-Botija, M., Petrucci, O., Pasqua, A.A., Rosselló, J., Vinet, F., Boissier, L., 2013. Towards a database on societal impact of Mediterranean floods within the framework of the HYMEX project. Nat. Hazards Earth Syst. Sci. 13 (5), 1337–1350. https://doi.org/10.5194/nhess-13-1337-2013.

Luke, S.H., Luckai, N.J., Burke, J.M., Prepas, E.E., 2007. Riparian areas in the Canadian boreal forest and linkages with water quality in streams. Environ. Rev. 15 (NA), 79–97. https://doi.org/10.1139/A07-001.

Lundin, L., 1982. Soil Moisture and Ground Water in Till Soil and the Significance of Soil Type for Runoff. Uppsala University, Uppsala.

Lupon, A., Bernal, S., Poblador, S., Martí, E., Sabater, F., 2016. The influence of riparian evapotranspiration on stream hydrology and nitrogen retention in a subhumid Mediterranean catchment. Hydrol. Earth Syst. Sci. 20 (9), 3831–3842. https://doi.org/10.5194/hess-20-3831-2016.

Lupon, A., Ledesma, J.L.J., Bernal, S., 2018. Riparian evapotranspiration is essential to simulate streamflow dynamics and water budgets in a Mediterranean catchment. Hydrol. Earth Syst. Sci. 22 (7), 4033–4045. https://doi.org/10.5194/hess-22-4033-2018.

Matheny, A.M., Bohrer, G., Stoy, P.C., Baker, I.T., Black, A.T., Desai, A.R., Dietze, M.C., Gough, C.M., Ivanov, V.Y., Jassal, R.S., Novick, K.A., Schäfer, K.V.R., Verbeeck, H., 2014. Characterizing the diurnal patterns of errors in the prediction of evapotranspiration by several land-surface models: An NACP analysis. J. Geophys. Res.-Biogeosci. 119 (7), 1458–1473. https://doi.org/10.1002/2014JG002623.

McClain, M.E., Boyer, E.W., Dent, C.L., Gergel, S.E., Grimm, N.B., Groffman, P.M., Hart, S.C., Harvey, J.W., Johnston, C.A., Mayorga, E., McDowell, W.H., Pinay, G., 2003. Biogeochemical hot spots and hot moments at the interface of terrestrial and aquatic ecosystems. Ecosystems 6 (4), 301–312. https://doi.org/10.1007/s10021-003-0161-9.

McDonnell, J.J., McGlynn, B.L., Kendall, K., Shanley, J., Kendall, C., 1998. The role of near-stream riparian zones in the hydrology of steep upland catchments. In: Kovar, K., Tappeiner, U., Peters, N.E., Craig, R.G. (Eds.), Hydrology. Iahs Publication, Water Resources and Ecology in Headwaters, pp. 173–180.

McDowell, W.H., Bowden, W.B., Asbury, C.E., 1992. Riparian nitrogen dynamics in two geomorphologically distinct tropical rain-forest watersheds: subsurface solute patterns. Biogeochemistry 18 (2), 53–75. https://doi.org/10.1007/bf00002703.

McGlynn, B.L., McDonnell, J.J., 2003. Quantifying the relative contributions of riparian and hillslope zones to catchment runoff. Water Resour. Res. 39 (11) https://doi.org/10.1029/2003wr002091.

Musolff, A., Fleckenstein, J.H., Opitz, M., Büttner, O., Kumar, R., Tittel, J., 2018. Spatio-temporal controls of dissolved organic carbon stream water concentrations. J. Hydrol. 566, 205–215. https://doi.org/10.1016/j.jhydrol.2018.09.011.

Nash, J.E., Sutcliffe, J.V., 1970. River flow forecasting through conceptual models part I - a discussion of principles. J. Hydrol. 10 (3), 282–290.

Pascual, D., Pla, E., López-Bustins, J.A., Retana, J., Terradas, J., 2015. Impacts of climate change on water resources in the Mediterranean Basin: a case study in Catalonia, Spain. Hydrol. Sci. J.-J. Sci. Hydrol. 60 (12), 2132–2147. https://doi.org/10.1080/02626667.2014.947290.

Peñuelas, J., Boada, M., 2003. A global change-induced biome shift in the Montseny mountains (NE Spain). Glob. Chang. Biol. 9 (2), 131–140. https://doi.org/10.1046/j.1365-2486.2003.00566.x.

Poblador, S., Lupon, A., Sabaté, S., Sabater, F., 2017. Soil water content drives spatiotemporal patterns of CO2 and N2O emissions from a Mediterranean riparian forest soil. Biogeosciences 14 (18), 4195–4208. https://doi.org/10.5194/bg-14-4195-2017.

Poblador, S., Thomas, Z., Rousseau-Gueutin, P., Sabaté, S., Sabater, F., 2019. Riparian forest transpiration under the current and projected Mediterranean climate: effects on soil water and nitrate uptake. Ecohydrology 12 (1), 16. https://doi.org/10.1002/eco.2043.

Rodhe, A., 1989. On the generation of stream runoff in till soils. Nordic Hydrol. 20 (1), 1–8.

Schwab, M., Klaus, J., Pfister, L., Weiler, M., 2016. Diel discharge cycles explained through viscosity fluctuations in riparian inflow. Water Resour. Res. 52 (11), 8744–8755. https://doi.org/10.1002/wrcr.v52.1110.1002/2016WR018626.

Seibert, J., Grabs, T., Köhler, S., Laudon, H., Winterdahl, M., Bishop, K., 2009. Linking soil- and stream-water chemistry based on a Riparian flow-concentration integration model. Hydrol. Earth Syst. Sci. 13 (12), 2287–2297.

Ledesma, J.L.J., Lupon, A., Bernal, S., 2021. Hydrological responses to the extratropical cyclone Gloria in two contrasting Mediterranean catchments in Spain; the perennial Font del Regàs and the intermittent Fuirosos. In review.

Swanson, F.J., Gregory, S.V., Sedell, J.R., Campbell, A.G., 1982. Land-water Interactions: The Riparian Zone. USDA Forest Service.

Tank, S.E., Fellman, J.B., Hood, E., Kritzberg, E.S., 2018. Beyond respiration: controls on lateral carbon fluxes across the terrestrial-aquatic interface. Limnol. Oceanogr. Lett. 3 (3), 76–88. https://doi.org/10.1002/lol2.10065.

Teuling, A.J., de Badts, E.A.G., Jansen, F.A., Fuchs, R., Buitink, J., Hoek van Dijke, A.J., Sterling, S.M., 2019. Climate change, reforestation/afforestation, and urbanization impacts on evapotranspiration and streamflow in Europe. Hydrol. Earth Syst. Sci. 23 (9), 3631–3652. https://doi.org/10.5194/hess-23-3631-2019.

Vicente-Serrano, S.M., Gouveia, C., Camarero, J.J., Beguería, S., Trigo, R., Lopez-Moreno, J.I., Azorin-Molina, C., Pasho, E., Lorenzo-Lacruz, J., Revuelto, J., Moran-Tejeda, E., Sanchez-Lorenzo, A., 2013. Response of vegetation to drought time-scales across global land biomes. Proc. Natl. Acad. Sci. U.S.A. 110 (1), 52–57. https://doi.org/10.1073/pnas.1207068110.

Wang, K.C., Dickinson, R.E., Liang, S.L., 2012. Global atmospheric evaporative demand over and from 1973 to 2008. J. Clim. 25 (23), 8353–8361. https://doi.org/10.1175/jcli-d-11-00492.1.

Weyer, C., Peiffer, S., Lischeid, G., 2018. Stream water quality affected by interacting hydrological and biogeochemical processes in a riparian wetland. J. Hydrol. 563, 260–272. https://doi.org/10.1016/j.jhydrol.2018.05.067.

Yu, X., Lamačova, A., Duffy, C., Krám, P., Hruška, J., 2016. Hydrological model uncertainty due to spatial evapotranspiration estimation methods. Comput. Geosci. 90, 90–101. https://doi.org/10.1016/j.cageo.2015.05.006.